

Sub-Wavelength Passive Optical Isolators Using Photonic Structures Based on Weyl Semimetals

Viktar S. Asadchy,* Cheng Guo, Bo Zhao, and Shanhui Fan*

The paper presents the design of sub-wavelength high-performing nonreciprocal optical devices using recently discovered magnetic Weyl semimetals. These passive bulk topological materials exhibit anomalous Hall effect which results in magneto-optical effects that are orders of magnitude higher than those in conventional materials, without the need of any external magnetic bias. Two optical isolators of both Faraday and Voigt geometries are designed. The isolators have dimensions that are reduced by three orders of magnitude compared to conventional magneto-optical configurations. The designed structures demonstrate that the magnetic Weyl semimetals may open up new avenues in photonics for the design of various nonreciprocal components.

1. Introduction

Isolators are nonreciprocal devices that allow light propagation in one direction but block it in the opposite direction. They play a fundamental role in modern communication systems, being used, for example, for suppressing back reflection in lasers and reducing multipath interference in communication channels. The ultimate requirements for an ideal isolator device are high isolation, compact size, low insertion loss, large bandwidth, and the absence of active components and external magnetic field.

Isolation inherently requires breaking Lorentz reciprocity, which can be achieved by breaking time-reversal symmetry or exploiting nonlinear response.^{[1](§ XII),[2–4]} Traditionally, isolators are designed based on magneto-optical materials such as yttrium iron or terbium gallium garnets, biased by an external magnetic field which breaks time-reversal symmetry.^[5–7] Ferrite-based isolators at microwave frequencies typically have dimensions of the operational wavelength or smaller due to strong gyromagnetic resonances.^{[8](§ 9.4)} On the contrary, at optical frequencies nonreciprocity in ferrite results from the nonresonant (weak) electron cyclotron orbiting, yielding optical isolators designs with dimensions of thousands of the operational wavelength or larger.^{[5](§ 13.3)} The size can be

partially decreased using geometries based on ring resonators or Mach–Zehnder interferometers; however, it is still of the order of millimeters.^[9,10] Another alternative for the size reduction of magneto-optical isolators is the use of magnetic photonic crystals.^[11–15] Nevertheless, they require either strong and nonuniform magnetization that is difficult to realize, or narrow-band resonances.

As modern photonics requires ultimate miniaturization of optical components, in the last decades, significant efforts have been devoted to the design of compact optical isolators based on time-modulated^[16–20] and nonlinear^[21–24] sys-

tems. Additional advantage of these systems over conventional magneto-optical materials is that they do not require an external magnetic field, or generate a static magnetic field through their intrinsic magnetic moment. These magnetic fields could negatively influence the operation of other optical components located in the closed proximity to the isolator. Nevertheless, practical realization of time-modulated isolators remain very challenging since it requires active sources, while nonlinear isolators have intrinsic limitations on their operations due to dynamic reciprocity.^[24]


In this paper, we demonstrate that gigantic optical isolation can be achieved by designing photonic structures based on recently discovered Weyl semimetals.^[25–30] It is known that these bulk topological materials can exhibit simultaneously broadband and giant magneto-optical effect without an external magnetic bias. Moreover, Weyl semimetals can be antiferromagnetic, exhibiting zero magnetic moment,^[31–35] and hence does not generate an external magnetic field. Based on the giant optical nonreciprocity in Weyl semimetals, we propose two designs of isolators at mid-infrared wavelengths with Faraday and Voigt geometries, respectively. The Faraday isolator provides more than 40 dB isolation and 0.33 dB insertion loss with unprecedented sub-wavelength thickness of a quarter wavelength (excluding polarizers and antireflective coatings). The Voigt isolator provides around 31.5 dB isolation and 1.2 dB insertion loss with a thickness of 1.38 wavelength, without the need of additional polarizers and antireflective coatings. These results enable creation of a new generation of passive optical isolators with dimensions reduced by three orders of magnitude compared to the previous solutions.

2. Axion Electrodynamics of Weyl Semimetals

Weyl semimetals are a novel class of 3D gapless topological matter.^[28–30,36–39] They feature accidental degenerate Weyl

Dr. V. S. Asadchy, Dr. B. Zhao, Prof. S. Fan
Ginzton Laboratory and Department of Electrical Engineering
Stanford University
Stanford, CA 94305, USA
E-mail: asadchy@stanford.edu; shanhui@stanford.edu

C. Guo
Department of Applied Physics
Stanford University
Stanford, CA 94305, USA

 The ORCID identification number(s) for the author(s) of this article can be found under <https://doi.org/10.1002/adom.202000100>.

DOI: 10.1002/adom.202000100

nodes in their band structure that host chiral fermions and appear in pairs of opposite chirality.^[27] Each Weyl node acts as a source/drain of Berry curvature in momentum space. The nontrivial topology of the Weyl nodes leads to unique electronic and optical properties that have generated significant interest in both fundamental science and technology. In the context of photonic applications, Weyl semimetals have been proposed recently for generation of nonreciprocal surface plasmons and design of nonreciprocal thermal emitters.^[40–42]

For concreteness, we consider the simplest case of a magnetic Weyl semimetal that hosts two Weyl nodes of opposite chirality at the same energy with a momentum separation $2\hbar\mathbf{b}$. Such an ideal Weyl semimetal phase has been experimentally realized very recently in EuCd_2As_2 .^[43] For this semimetal, the electric permittivity assumes the form of the so-called axion electrodynamics^[44]:

$$\mathbf{D} = \varepsilon_d \mathbf{E} + \frac{ie^2}{4\pi^2\hbar\omega} 2\mathbf{b} \times \mathbf{E} \quad (1)$$

while $\mathbf{B} = \mu_0\mathbf{H}$ is not modified. Here, e is the electron charge, \hbar is the reduced Planck constant, ω is the angular frequency, and ε_d denotes the permittivity of the corresponding Dirac semimetal with doubly degenerate bands, which is assumed isotropic. The second term in Equation (1) describes the anomalous Hall effect in the dynamical regime, manifesting itself as the magneto-optical effect.^[45] The axial vector $2\mathbf{b}$ acts as an effective magnetic field. Its effect on the dielectric permittivity is similar to that of an external magnetic field on a plasmonic metal. In this case, however, \mathbf{b} is entirely due to the electronic structure of the Weyl semimetal, is entirely internally generated, and does not correspond to an external magnetic field. If we choose the crystal orientation of the Weyl semimetal such that \mathbf{b} is along the $\hat{\mathbf{z}}$ direction: $\mathbf{b} = b\hat{\mathbf{z}}$, the effective permittivity tensor in $\mathbf{D} = \bar{\varepsilon} \cdot \mathbf{E}$ becomes

$$\bar{\varepsilon} = \begin{pmatrix} \varepsilon_d & i\varepsilon_a & 0 \\ -i\varepsilon_a & \varepsilon_d & 0 \\ 0 & 0 & \varepsilon_d \end{pmatrix} \quad (2)$$

where $\varepsilon_a = be^2/(2\pi^2\hbar\omega)$. Thus, $\bar{\varepsilon}$ is asymmetric and breaks Lorentz reciprocity.^{[46](§ 5.5c)} The diagonal term ε_d is calculated by using the Kubo-Greenwood formalism within the random phase approximation to a two-band model with spin degeneracy^[40,44,47]:

$$\varepsilon_d = \varepsilon_b + \frac{ir_s g}{6\omega} \Omega G(\Omega/2) - \frac{r_s g}{6\pi\omega} \left\{ 4 \left[1 + \frac{\pi^2}{3} \left(\frac{k_B T}{E_F(T)} \right)^2 \right] + 8\Omega \int_0^\xi \frac{G(\xi) - G(\Omega/2)}{\Omega^2 - 4\xi^2} \xi d\xi \right\} \quad (3)$$

here ε_b is the background permittivity, E_F is the chemical potential, $\Omega = \hbar(\omega + i\tau^{-1})/E_F$ is the normalized complex frequency, τ^{-1} is the Drude damping rate, $G(E) = n(-E) - n(E)$, where $n(E)$ is the Fermi distribution function, $r_s = e^2/(4\pi\epsilon_0\hbar v_F)$ is the effective fine-structure constant, v_F is the Fermi velocity, g is the number of Weyl points, and $\xi_c = E_c/E_F$, where E_c is the cutoff

energy beyond which the band dispersion is no longer linear.^[47] Following,^[40] in this work we use the parameters $\varepsilon_b = 6.2$, $\xi_c = 3$, $\tau = 1000$ fs, $g = 2$, $b = 8.5 \times 10^8$ m⁻¹, $v_F = 0.83 \times 10^5$ m s⁻¹, and $E_F = 0.30$ eV at $T = 300$ K.

Figure 1b (upper plot) depicts frequency dispersion of permittivity components ε_d and ε_a . It is seen that ε_a is comparable to ε_d over a broad wavelength range. This dispersion indicates strong nonreciprocity in Weyl semimetals characterized with the magneto-optical parameter^[5] $Q \equiv \varepsilon_a/\varepsilon_d \approx 1$, which is around three orders of magnitude larger than that of conventional magneto-optical materials in the optical frequencies with $Q \approx 10^{-3}$.^[5] Such a strong nonreciprocity is induced by the intrinsic Berry curvature in Weyl semimetals. It is naturally broadband, in sharp contrast to the magneto-optical effects induced by Zeeman splitting in two-level systems.^[48] It can appear in the absence of an external magnetic field. Moreover, the magnetic Weyl semimetal can be antiferromagnetic,^[31,32] that is, exhibit zero net magnetic moment. Antiferromagnetic nonreciprocal optical devices will benefit integrated optoelectronics as they do not generate net magnetic field outside, which would otherwise interfere with other adjacent components.

3. Design of Optical Isolators Based on Weyl Semimetals

The giant nonreciprocity in magnetic Weyl semimetals results in significant magneto-optical effects, in both the Faraday geometry where the light travels along the Weyl node separation ($\mathbf{k} \parallel \mathbf{b}$), and the Voigt geometry where the light travels perpendicularly to the Weyl node separation ($\mathbf{k} \perp \mathbf{b}$).^[5] Here \mathbf{k} denotes the wavevector of light.

First, we consider the Faraday geometry: For linearly polarized light propagating in the Weyl semimetal along \mathbf{b} direction, the plane of polarization is rotated by the angle^{[5](§ 3.1)}

$$\theta_F = V_W(\omega)L = \text{Re}(n_- - n_+) \frac{\omega}{2c} L \quad (4)$$

where $V_W(\omega)$ is the modified Verdet coefficient defined as rotation per unit path, L is the light propagation distance inside Weyl semimetal, c is speed of light in vacuum, $n_+ = \sqrt{\varepsilon_d - \varepsilon_a}$ and $n_- = \sqrt{\varepsilon_d + \varepsilon_a}$ are the refractive indices for right and left circularly polarized light, respectively. The angle θ_F is counted from the x axis toward the y axis. We have calculated the modified Verdet coefficient for the Weyl semimetal (see Supporting Information § 1). The maximum V_W reaches 1.67 rad/ μm at 4 μm . For comparison, to reach such an value at this wavelength using conventional magneto-optical material such as YbBi:YIG , one needs to apply an impractical external magnetic field that exceeds 300 T. Moreover, compared to the giant Faraday rotation, the attenuation can be moderate in Weyl semimetals. As a figure of merit, the dimensionless ratio of the Verdet coefficient and the attenuation coefficient for linearly polarized light $V_W/\alpha \approx 13$ near wavelength of 4 μm (see Supporting Information § 1). Therefore, it is possible to design an isolator with low insertion loss based on Weyl semimetals.

The geometry of the designed Faraday isolator based on Weyl semimetal is shown in Figure 1a. The semimetal slab of thickness L is encompassed by two linear polarizers twisted at 45°.

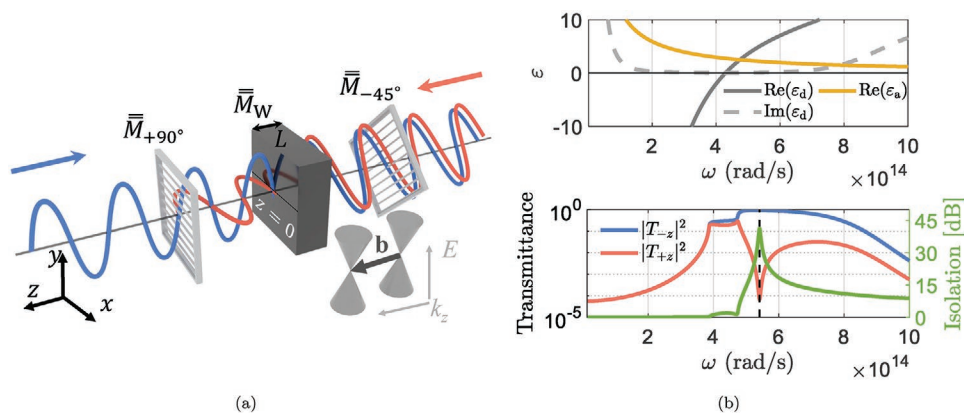


Figure 1. a) Geometry of the Faraday isolator based on Weyl semimetal slab of thickness L and Weyl nodes separation in the momentum space \mathbf{b} . The inset shows the bulk energy E dispersion of the semimetal. The silver grids depict linear polarizers. The red and blue traces denote the electric fields of linearly polarized waves propagating, respectively, along the $-z$ - and $+z$ -directions. Matrices \bar{M}_{+90° , \bar{M}_{-45° , and \bar{M}_W stand for the Jones matrices of the two polarizers and the Weyl semimetal slab. b) Top: Angular frequency dispersion of the permittivity components of bulk Weyl semimetal with the parameters defined in the main text. Bottom: Transmittances for waves travelling through the Weyl isolator along $\pm z$ -directions with polarization states shown in (a). The blue and red colors in (a) and (b) correspond to the same waves. The green curve shows the isolation ratio. The dashed line depicts the frequency of the highest isolation.

The left interface of the slab is located at $z = 0$, while the right one at $z = -L$. For this example, we assume that reflections at the interface between Weyl semimetal and free space can be suppressed by adding antireflective coatings at the two sides of the slab.

Figure 1b (bottom plot) depicts the calculated transmittance for both illuminations of the Weyl isolator with a thickness $L = 0.886 \mu\text{m}$ using Jones matrix analysis (see Supporting Information § 2). At an angular frequency $\omega = 5.41 \times 10^{14} \text{ rad s}^{-1}$ ($\lambda = 3.5 \mu\text{m}$), the isolation reaches the maximum value of 41.3 dB supported by very low insertion loss of 0.33 dB. Importantly, such great isolation property occurs for the Weyl slab of extraordinary small thickness of $L = 0.25\lambda$. For comparison, an optical isolator based on garnet YbBi:YIG at the same wavelength must have thickness of at least $L = 150 \mu\text{m}$ when biased by an external magnetic field $B_0 = 1 \text{ T}$. The sub-wavelength thickness of the Weyl isolator and the absence of the external bias make it very appealing candidate for future photonics applications.

Next, we consider the Voigt geometry, which is of interest for several reasons. First, the relative orientation of the Weyl node separation with respect to the crystal surface depends on the specific material and the growth condition. Thus, in some cases vector \mathbf{b} is restricted to be parallel to the film surface. Second, Voigt isolators do not require additional polarizers or antireflective coating used in Faraday geometry, and hence may be simpler in implementation. Voigt isolators based on conventional magneto-optical materials have been proposed using one-dimensional photonic crystal structures.^[12–14] Due to the weak nonreciprocity in conventional magneto-optical materials, as many as 50 unit cells of the photonic crystal are needed to realize optical isolation.

Here we show that the use of Weyl semimetal can lead to far more compact Voigt isolators. For this purpose, we consider a finite 1D photonic crystal structure incorporating alternating layers of Weyl semimetals with \mathbf{b} vector parallel to the layers

and isotropic dielectric films. We determine the simplest configuration of the primitive cell of the photonic crystal by symmetry considerations. The spectral nonreciprocity, that is, $\omega(\mathbf{k}) \neq \omega(-\mathbf{k})$, requires that the magnetic symmetry group G of the structure must not include any element $g \in G$ that flips the wavevector, that is, $\forall g \in G, g\mathbf{k} \neq -\mathbf{k}$.^[49] It follows that for the materials we consider (Weyl semimetal and isotropic dielectric), the simplest primitive cell must consist of three layers, since with the materials that we assume here, any infinite 1D photonic crystal with a unit cell containing two layers always maintains spatial inversion symmetry $\mathcal{I}\mathbf{k} = -\mathbf{k}$. We note that a finite 1D crystal with two layers per unit cell may break inversion symmetry, and thus exhibit nonreciprocal behavior due to time-reversal symmetry breaking in the Weyl semimetal; however, the nonreciprocal effect is usually weak (see Supporting Information § 3). As for photonic crystals with three layers per unit cell, there are two possible configurations. The first configuration consists of two different dielectric layers and single Weyl semimetal layer in the primitive cell, which is examined in Supporting Information § 6. The second configuration consists of two Weyl layers and one dielectric layer, which exhibits the best characteristics in terms of the isolation and compactness and is considered below.

Figure 2a depicts the geometry of the proposed Voigt isolator. The unit cell comprises two semimetal layers with opposite in-plane Weyl nodes separations \mathbf{b} and a dielectric layer made of fused silica with permittivity dispersion $\epsilon_2(\omega)$ measured in ref. [50]. The Weyl layers have the same thickness of $x_1 = x_3 = 480 \text{ nm}$, while the thickness of the dielectric layer is $x_2 = 1.44 \mu\text{m}$. The total unit cell size is $\Lambda = x_1 + x_2 + x_3 = 2.4 \mu\text{m}$. We consider off-normal incidence since the crystal is reciprocal for normal incidence (see Supporting Information § 3). Using the transfer matrix method,^[51] we calculate the band structure of an infinite photonic crystal and the transmission spectrum of a finite structure (see more details in Supporting Information § 4). Figure 2b depicts the projected band structure for an

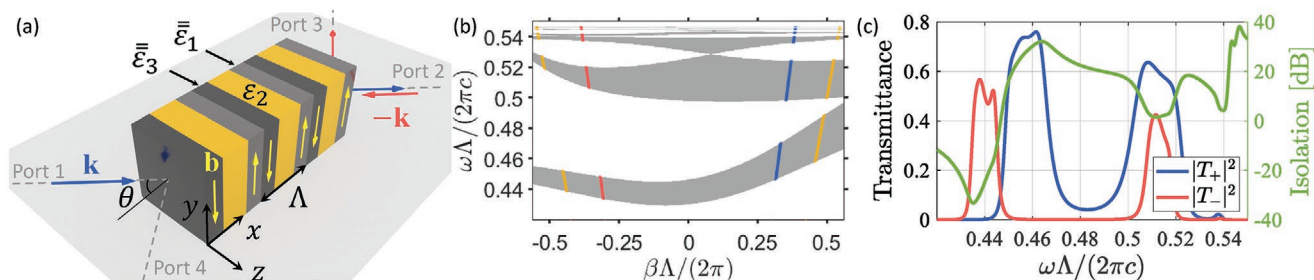


Figure 2. a) Geometry of the Weyl photonic crystal with the unit cell comprising three layers. The materials of the dark and bright grey layers are Weyl semimetals with opposite node separation shown by the yellow arrows. The dielectric films are shown in yellow. The blue and red arrows depict forward and backward illuminations, respectively. b) Projected band structure of an infinite Weyl photonic crystal shown in (a). Here, β denotes the wavevector components parallel to the layers. The gray regions indicate the allowed bands. The yellow color denotes the light lines, while the blue and red vertical lines indicate dispersion relations for forward and backward incidence at $\theta = 45.6^\circ$, respectively. c) Transmittances and isolation ratio for the forward and backward illuminations of the photonic crystal.

infinite crystal with respect to the $k_z = \beta$ component of incident wavevectors, where the gray and white regions illustrate the allowed and forbidden bands, respectively. Such projected band structure is highly asymmetric with respect to β , which is expected to lead to nonreciprocal transmission for a finite structure. Figure 2c depicts the transmittance spectra of a finite structure with three unit cells for the two opposite illuminations with wavevectors \mathbf{k} and $-\mathbf{k}$ at an incident angle $\theta = 45.6^\circ$. The isolation ratio reaches 31.5 dB with an insertion loss of 1.2 dB at $\omega = 0.4619 \times 2\pi c/\Lambda$ ($\lambda = 5.2 \mu\text{m}$). We note that this frequency is below the bulk plasmon frequency, meaning that the high transmission in the forward direction is analogous to the effect of the wave tunnelling in single-negative materials.^[52] Remarkably, the high isolation ratio is achieved with the total thickness $3\Lambda = 7.2 \mu\text{m} = 1.38 \lambda$. Plots of reflectance spectra can be found in Supporting Information § 5. Interestingly, this device operates as an optical circulator with four ports shown in Figure 2a. The nonreciprocal wave propagation paths of this circulator are $1 \rightarrow 2$, $2 \rightarrow 3$, $3 \rightarrow 4$, and $4 \rightarrow 1$, where the numbers correspond to the ports. Similar functionality was previously achieved, for example, in ref. [53], using conventional magneto-optical materials together with additional elements, such as quartz rotator, the Rochon prism, and mirrors. Our construction here is far simpler. In the above analysis, we assumed that the Weyl optical isolator is at room temperature ($T = 300 \text{ K}$). Detailed discussion on the performance of the isolator at different temperature regimes can be found in Supporting Information § 7.

Our designs above utilize the giant nonreciprocity associated with the bulk conductivity $\bar{\sigma}_B$ of Weyl semimetals. Weyl semimetals also feature topological Fermi arc surface states when \mathbf{b} has components parallel to the surface, such as in the Voigt geometry.^[54] Such surface states lead to a surface conductivity $\bar{\sigma}_S$, which modifies the boundary conditions for electromagnetic waves: $\hat{\mathbf{y}} \cdot [\mathbf{H}(x+0) - \mathbf{H}(x-0)] = \hat{\mathbf{y}} \cdot \bar{\sigma}_S \cdot \mathbf{E}(x)$. In our calculation, we neglect the surface term on the right side of this equation. This is because the relative importance of the bulk and surface terms is determined by the magnitudes of $\bar{\sigma}_B$ and $k\bar{\sigma}_S$. We numerically verified that in the frequency and wavevector regime of isolation operation, for a typical surface conductivity $\sigma_S \approx e^2/h$,^[55] $k\bar{\sigma}_S \ll \bar{\sigma}_B$ and the surface term $\hat{\mathbf{y}} \cdot \bar{\sigma}_S \cdot \mathbf{E}(x) < 0.01 \cdot H_y(x)$, thus is negligible.

4. Conclusion

Despite the explosive growth of research on Weyl semimetals in condensed matter, its applications for photonics are yet to be explored. The above two examples of compact optical isolators clearly demonstrate that magnetic Weyl semimetals provide unprecedented material response that will open up new avenues for the design of nonreciprocal components. The absence of the external bias field and the subwavelength dimensions provide Weyl semimetal-based nonreciprocal optical components with unique advantages as compared with those based on magneto-optical or time-modulation effects. Similarly to the many applications enabled by the discovery of graphene, its 3D analogue, Weyl semimetal, may also lead to useful and novel photonic devices.

Supporting Information

Supporting Information is available from the Wiley Online Library or from the author.

Acknowledgements

V.S.A. and C.G. contributed equally to this work. This work was supported in part by the Finnish Foundation for Technology Promotion and by the U.S. Air Force Office of Scientific Research Grant No. FA9550-18-1-0379.

Conflict of Interest

The authors declare no conflict of interest.

Keywords

anomalous Hall effect, Faraday effect, isolators, nonreciprocity, photonic crystals, topological materials, Weyl semimetals

Received: January 16, 2020

Revised: April 16, 2020

Published online:

- [1] L. D. Landau, E. M. Lifshitz, *Statistical Physics, part 1 (Course of Theoretical Physics)*, Vol. 5, Elsevier, Oxford **1980**.
- [2] D. Jalas, A. Petrov, M. Eich, W. Freude, S. Fan, Z. Yu, R. Baets, M. Popović, A. Melloni, J. D. Joannopoulos, M. Vanwolleghem, C. R. Doerr, H. Renner, *Nat. Photonics* **2013**, *7*, 579.
- [3] C. Caloz, A. Alù, S. Tretyakov, D. Sounas, K. Achouri, Z.-L. Deck-Léger, *Phys. Rev. Appl.* **2018**, *10*, 047001.
- [4] V. Asadchy, M. S. Mirmoosa, A. Díaz-Rubio, S. Fan, S. A. Tretyakov, *arXiv:2001.04848* **2020**.
- [5] A. K. Zvezdin, V. A. Kotov, *Modern Magneto-optics and Magneto-optical Materials*, CRC Press, Boca Raton **1997**.
- [6] J. Fujita, M. Levy, R. M. Osgood, L. Wilkens, H. Dötsch, *Appl. Phys. Lett.* **2000**, *76*, 2158.
- [7] Y. Shoji, T. Mizumoto, H. Yokoi, I.-W. Hsieh, R. M. Osgood, *Appl. Phys. Lett.* **2008**, *92*, 071117.
- [8] D. M. Pozar, *Microwave Engineering*, John Wiley & Sons, New York **2012**.
- [9] Q. Du, C. Wang, Y. Zhang, Y. Zhang, T. Fakhrlul, W. Zhang, C. Gonçalves, C. Blanco, K. Richardson, L. Deng, C. A. Ross, L. Bi, J. Hu, *ACS Photonics* **2018**, *5*, 5010.
- [10] Y. Zhang, Q. Du, C. Wang, T. Fakhrlul, S. Liu, L. Deng, D. Huang, P. Pintus, J. Bowers, C. A. Ross, J. Hu, L. Bi, *Optica* **2019**, *6*, 473.
- [11] A. Figotin, I. Vitebsky, *Phys. Rev. E* **2001**, *63*, 066609.
- [12] I. L. Lyubchanskii, N. N. Dadoenkova, M. I. Lyubchanskii, E. A. Shapovalov, T. Rasing, *J. Phys. D: Appl. Phys.* **2003**, *36*, R277.
- [13] Z. Yu, Z. Wang, S. Fan, *Appl. Phys. Lett.* **2007**, *90*, 121133.
- [14] A. B. Khanikaev, M. J. Steel, *Opt. Express* **2009**, *17*, 5265.
- [15] K. Fang, Z. Yu, V. Liu, S. Fan, *Opt. Lett.* **2011**, *36*, 4254.
- [16] A. L. Cullen, *Nature* **1958**, *181*, 332.
- [17] Z. Yu, S. Fan, *Nat. Photonics* **2009**, *3*, 91.
- [18] H. Lira, Z. Yu, S. Fan, M. Lipson, *Phys. Rev. Lett.* **2012**, *109*, 033901.
- [19] K. Fang, Z. Yu, S. Fan, *Phys. Rev. Lett.* **2012**, *108*, 153901.
- [20] D. L. Sounas, A. Andrea, *Nat. Photonics* **2017**, *11*, 774.
- [21] M. D. Tocci, M. J. Bloemer, M. Scalora, J. P. Dowling, C. M. Bowden, *Appl. Phys. Lett.* **1995**, *66*, 2324.
- [22] B. Peng, Ş. K. Özdemir, F. Lei, F. Monifi, M. Gianfreda, G. L. Long, S. Fan, F. Nori, C. M. Bender, L. Yang, *Nat. Phys.* **2014**, *10*, 394.
- [23] L. Fan, J. Wang, L. T. Varghese, H. Shen, B. Niu, Y. Xuan, A. M. Weiner, M. Qi, *Science* **2012**, *335*, 447.
- [24] Y. Shi, Z. Yu, S. Fan, *Nat. Photonics* **2015**, *9*, 388.
- [25] P. Hosur, X. Qi, *C. R. Phys.* **2013**, *14*, 857.
- [26] B. Yan, C. Felser, *Annu. Rev. Condens. Matter Phys.* **2017**, *8*, 337.
- [27] N. P. Armitage, E. J. Mele, A. Vishwanath, *Rev. Mod. Phys.* **2018**, *90*, 015001.
- [28] I. Belopolski, K. Manna, D. S. Sanchez, G. Chang, B. Ernst, J. Yin, S. S. Zhang, T. Cochran, N. Shumiya, H. Zheng, B. Singh, G. Bian, D. Multer, M. Litskevich, X. Zhou, S.-M. Huang, B. Wang, T.-R. Chang, S.-Y. Xu, A. Bansil, C. Felser, H. Lin, M. Z. Hasan, *Science* **2019**, *365*, 1278.
- [29] N. Morali, R. Batabyal, P. K. Nag, E. Liu, Q. Xu, Y. Sun, B. Yan, C. Felser, N. Avraham, H. Beidenkopf, *Science* **2019**, *365*, 1286.
- [30] D. F. Liu, A. J. Liang, E. K. Liu, Q. N. Xu, Y. W. Li, C. Chen, D. Pei, W. J. Shi, S. K. Mo, P. Dudin, T. Kim, C. Cacho, G. Li, Y. Sun, L. X. Yang, Z. K. Liu, S. S. P. Parkin, C. Felser, Y. L. Chen, *Science* **2019**, *365*, 1282.
- [31] H. Yang, Y. Sun, Y. Zhang, W.-J. Shi, S. S. P. Parkin, B. Yan, *New J. Phys.* **2017**, *19*, 015008.
- [32] Y. Zhang, Y. Sun, H. Yang, J. Železný, S. P. P. Parkin, C. Felser, B. Yan, *Phys. Rev. B* **2017**, *95*, 075128.
- [33] S. Chowdhury, K. F. Garrity, F. Tavazza, *npj Comput. Mater.* **2019**, *5*, 33.
- [34] M. M. Otrokov, I. P. Rusinov, M. Blanco-Rey, M. Hoffmann, A. Y. Vyazovskaya, S. V. Ereemeev, A. Ernst, P. M. Echenique, A. Arnau, E. V. Chulkov, *Phys. Rev. Lett.* **2019**, *122*, 107202.
- [35] M. M. Otrokov, I. I. Klimovskikh, H. Bentmann, D. Estyunin, A. Zeugner, Z. S. Aliev, S. Gaß, A. U. B. Wolter, A. V. Koroleva, A. M. Shikin, M. Blanco-Rey, M. Hoffmann, I. P. Rusinov, A. Y. Vyazovskaya, S. V. Ereemeev, Y. M. Koroteev, V. M. Kuznetsov, F. Freyse, J. Sánchez-Barriga, I. R. Amiraslanov, M. B. Babanly, N. T. Mamedov, N. A. Abdullayev, V. N. Zverev, A. Alfonso, V. Kataev, B. Büchner, E. F. Schwier, S. Kumar, A. Kimura, L. Petaccia, G. Di Santo, R. C. Vidal, S. Schatz, K. Kißner, M. Ünzelmann, C. H. Min, S. Moser, T. R. F. Peixoto, F. Reinert, A. Ernst, P. M. Echenique, A. Isaeva, E. V. Chulkov, *Nature* **2019**, *576*, 416.
- [36] S.-Y. Xu, I. Belopolski, N. Alidoust, M. Neupane, G. Bian, C. Zhang, R. Sankar, G. Chang, Z. Yuan, C.-C. Lee, S.-M. Huang, H. Zheng, J. Ma, D. S. Sanchez, B. Wang, A. Bansil, F. Chou, P. P. Shibayev, H. Lin, S. Jia, M. Z. Hasan, *Science* **2015**, *349*, 613.
- [37] B. Q. Lv, H. M. Weng, B. B. Fu, X. P. Wang, H. Miao, J. Ma, P. Richard, X. C. Huang, L. X. Zhao, G. F. Chen, Z. Fang, X. Dai, T. Qian, H. Ding, *Phys. Rev. X* **2015**, *5*, 031013.
- [38] K. Kuroda, T. Tomita, M.-T. Suzuki, C. Bareille, A. A. Nugroho, P. Goswami, M. Ochi, M. Ikhlas, M. Nakayama, S. Akebi, R. Noguchi, R. Ishii, N. Inami, K. Ono, H. Kumigashira, A. Varykhalov, T. Muro, T. Koretsune, R. Arita, S. Shin, T. Kondo, S. Nakatsuji, *Nat. Mater.* **2017**, *16*, 1090.
- [39] M. Hirschberger, S. Kushwaha, Z. Wang, Q. Gibson, S. Liang, C. A. Belvin, B. A. Bernevig, R. J. Cava, N. P. Ong, *Nat. Mater.* **2016**, *15*, 1161.
- [40] O. V. Kotov, Y. E. Lozovik, *Phys. Rev. B* **2018**, *98*, 195446.
- [41] B. Zhao, C. Guo, C. A. C. Garcia, P. Narang, S. Fan, *Nano Lett.* **2020**, *20*, 1923.
- [42] Y. Tsurimaki, X. Qian, S. Pajovic, F. Han, M. Li, G. Chen, *Phys. Rev. B* **2020**, *101*, 165426.
- [43] J.-R. Soh, F. de Juan, M. G. Vergniory, N. B. M. Schröter, M. C. Rahn, D. Y. Yan, J. Jiang, M. Bristow, P. A. Reiss, J. N. Blandy, Y. F. Guo, Y. G. Shi, T. K. Kim, A. McCollam, S. H. Simon, Y. Chen, A. I. Coldea, A. T. Boothroyd, *Phys. Rev. B* **2019**, *100*, 201102.
- [44] J. Hofmann, S. Das Sarma, *Phys. Rev. B* **2016**, *93*, 241402.
- [45] N. Nagaosa, J. Sinova, S. Onoda, A. H. MacDonald, N. P. Ong, *Rev. Mod. Phys.* **2010**, *82*, 1539.
- [46] J. A. Kong, *Electromagnetic Wave Theory*, Wiley, New York **1986**.
- [47] O. V. Kotov, Y. E. Lozovik, *Phys. Rev. B* **2016**, *93*, 235417.
- [48] L. Ying, M. Zhou, X. Luo, J. Liu, Z. Yu, *Optica* **2018**, *5*, 1156.
- [49] I. Vitebsky, J. Edelkind, E. N. Bogachek, A. G. Scherbakov, U. Landman, *Phys. Rev. B* **1997**, *55*, 12566.
- [50] L. H. Malitson, *J. Opt. Soc. Am.* **1965**, *55*, 1205.
- [51] P. Yeh, A. Yariv, C.-S. Hong, *J. Opt. Soc. Am.* **1977**, *67*, 423.
- [52] H. Jiang, H. Chen, H. Li, Y. Zhang, J. Zi, S. Zhu, *Phys. Rev. E* **2004**, *69*, 066607.
- [53] K. Kobayashi, M. Seki, *IEEE J. Quantum Electron.* **1980**, *16*, 11.
- [54] I. Belopolski, S.-Y. Xu, D. S. Sanchez, G. Chang, C. Guo, M. Neupane, H. Zheng, C.-C. Lee, S.-M. Huang, G. Bian, N. Alidoust, T.-R. Chang, B. Wang, X. Zhang, A. Bansil, H.-T. Jeng, H. Lin, S. Jia, M. Z. Hasan, *Phys. Rev. Lett.* **2016**, *116*, 066802.
- [55] Q. Chen, A. R. Kutayiah, I. Oladyskhin, M. Tokman, A. Belyanin, *Phys. Rev. B* **2019**, *99*, 075137.